Environmental Science & Technology

Article

Cite This: Environ. Sci. Technol. 2019, 53, 9328−9336

pubs.acs.org/est

CO_2/CH_4 Competitive Adsorption in Shale: Implications for Enhancement in Gas Production and Reduction in Carbon Emissions

Jun Liu,*[,†,∥] Lingzhi Xie,[†] Derek Elsworth,[‡] and Quan Gan[§]

[†]Key Laboratory of Deep Underground Science and Engineering (Ministry of Education), Institute of New Energy and Low-Carbon Technology, Sichuan University, Chengdu 610065, China

[‡]Department of Energy and Mineral Engineering, Pennsylvania State University, University Park, Pennsylvania 16802, United States

[§]Department of Petroleum Geology & Geology, School of Geosciences, University of Aberdeen, AB24 3UE, Aberdeen, U.K.

Supporting Information

ABSTRACT: CO_2/CH_4 interaction determines the prospects for complementary enhanced gas recovery (EGR) associated with CO_2 sequestration in shale. We characterize the competitive adsorption of CO_2 and CH_4 in shale using low-field NMR. Competitive sorption of CO_2 relative to CH_4 is defined as the CO_2/CH_4 competitive adsorption ratio (CO_2/CH_4 CAR for short) when CO_2 and CH_4 have the same original partial pressure in shale. Results indicate the CO_2/CH_4 CAR decreases with the logarithm of increasing pressure. Observed CO_2/CH_4 CARs are on the order of 4.28−5.81 (YDN-1) to 3.43−5.57 (YDN-2), describing the remarkable competitive advantage of CO_2 sorption relative to CH_4 for shale. Results also indicate that increasing the CO_2/CH_4 pressure ratio (1) increases the adsorption capacity of shales to CO_2 and decreases that to CH_4 logarithmically with pressure, and (2) boosts CO_2−CH_4 displacement and generates greater EGR efficiency in shale, where the EGR efficiency can be inferred by the CO_2/CH_4 pressure ratio using a Langmuir-like function. Furthermore, the maximum sequestration capacity of adsorbed CO_2 during CO_2−CH_4 competition is on the order of ∼3.87 cm^3/g (YDN-1) to ∼5.13 cm^3/g (YDN-2). These promising results for EGR and CO_2 storage reveal the considerable potential for carbon capture and geological sequestration in shale.

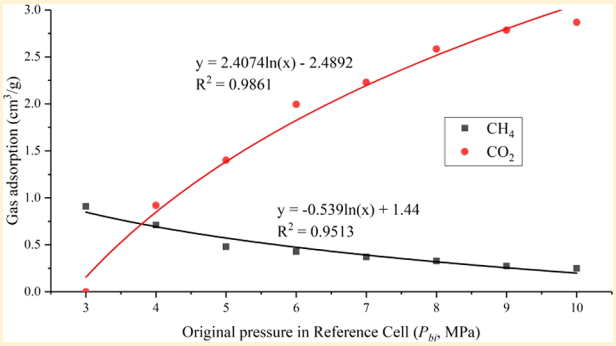

1. INTRODUCTION

CO_2 injection into shale has hitherto been lauded as a potentially effective and promising technique capable of concurrently sequestering carbon through carbon capture and geological sequestration (CCGS) while stimulating enhanced production of methane from shale.[1−5] The mechanism of CCGS in shale is the displacement of originally adsorbed CH_4 when CO_2 is injected into the gas shale.[6,7] In other words, the differential adsorption potential in shale for CO_2 and CH_4 results in this enhanced gas recovery (EGR).[8,9] Thus, accurately defining the competitive adsorption behavior between CO_2 and CH_4 in shale is a necessary requirement in designing shale-based CCGS techniques.

To date, the adsorption behavior of CO_2 and CH_4 in shale has been investigated using a variety of experimental measurements and numerical or molecular simulations. Numerical and molecular simulations are beneficial for assessing EGR efficiency and CO_2 storage capacity in shale and for evaluating the influence of reservoir characteristics on the adsorption behavior of CO_2 and CH_4.[10,11] Some simulations note a 7% incremental increase in gas production with a theoretical maximum CO_2 storage capacity of 1.6 Mt/km^2 for the Marcellus shale in the eastern United States, based on the Langmuir volume from adsorption isotherm.[8] Molecular simulations suggest optimal operating conditions at a depth of 1 km for the displacement of CH_4 by CO_2 in shale.[12] Molecular simulations also indicate that the kerogen derived from higher plants is the optimal organic type for shale-based CCGS and that reservoir moisture boosts EGR efficiency in shale.[13] However, numerical and molecular studies generally rely on simplified reservoir models or assumptions and thus represent only broad constraints on the realistic interaction between CO_2 and CH_4 in shale.

Compared with numerical and molecular simulations, experimental measurements directly define the real interplay between CO_2 and CH_4 in shale and define adsorption isotherms that are widely adopted.[14−16] On the basis of adsorption isotherms, Nuttall et al.[17] investigated Devonian shale from Kentucky and found ratios of adsorbed CO_2 relative to CH_4 on the order of 5 to 1, whereas Chareonsuppanimit et al.[18] observed ratios of adsorbed CO_2/CH_4 closer to 3 to 1 at pressures of ∼7 MPa for the New Albany shale from the Illinois basin. Increasing temperature and CO_2 content in the

Received: April 22, 2019
Revised: July 15, 2019
Accepted: July 18, 2019
Published: July 18, 2019

DOI: 10.1021/acs.est.9b02432
Environ. Sci. Technol. 2019, 53, 9328−9336

CO_2/CH_4 mixture are also observed to promote preferential sorption of CO_2, according to the sorption isotherms of pure CH_4, CO_2 and mixed CO_2/CH_4.[16] Unfortunately, adsorption isotherms of CO_2, CH_4 or CO_2/CH_4 mixtures are usually performed separately in laboratory analyses (e.g., volumetric or gravimetric methods) that are incapable of defining competitive adsorption (between CO_2 and CH_4).[19] Furthermore, few robust methods are able to identify the adsorption capacity of multiple components from a CO_2/CH_4 mixture. As a result, quantitative characterizations of the competitive interaction between CO_2 and CH_4 in shale are rare.

As verified by Liu et al.[20] and Yao et al.,[21] low-field nuclear magnetic resonance (NMR) has the capability to identify adsorbed CH_4 concentrations in shale. Accordingly, on the basis of low-field NMR theory, this study creatively develops a systemic strategy to measure the adsorption capacity of multiple components from a CO_2/CH_4 mixture. This new proposal is a direct experimental method and aims at monitoring and quantifying the competitive adsorption behavior of CO_2 and CH_4 in real time under a realistic environment with complicated pore systems in shale to provide important new data. Furthermore, this study discusses the potential efficiency of EGR and the capacity for CO_2 sequestration in shale during CO_2/CH_4 competitive adsorption. Considering that CO_2 injection into shale is a promising technique applicable to the CCGS technique, this study should have significant implications for research on CO_2 emission reduction, as well as on production enhancement of shale gas.

2. MATERIALS AND ANALYTICAL METHODOLOGY

We sample two shales and expose these samples in a unique NMR device that creates constant temperature and variable pressures. Transverse relaxation times (T_2) are measured and used to determine isotherms as gas pressures are varied in the shale samples. These experiments quantify the adsorptive competition between CH_4 and CO_2 and explore EGR efficiency and CO_2 sequestration capacity in shales.

2.1. Shale Samples and Pretreatment. In this study, two organic-rich shale samples were collected from the lower Silurian Longmaxi formation in the southeastern Sichuan basin, China. This specified formation originated from typical marine sediments with thicknesses ranging from 40 to 110 m.[22] The Longmaxi formation is generally divided into two members: the lower member (deposited in a deep-water shelf environment) and the upper member (deposited in a shallow-water shelf environment).[22] Described as carbonaceous shale, the two shale samples were collected from the lower member. Samples YDN-1 and YDN-2 were obtained from a shale gas exploration well at depths of 698 and 747 m, respectively. So far, the Longmaxi formation is the main target for commercial shale gas extraction in China, suggesting that the samples used in this study are representative of commercially viable reservoirs.

Both samples are characterized as low porosity and permeability, overmature (as exhibited by R_o) and high total organic carbon (TOC) content shales (Supporting Information (SI), Table S1). Minerals in the study samples are predominantly quartz and clay, supplemented with carbonate minerals, feldspar and pyrite that account for <20% of the composition (SI Table S1). In addition, the results from the low-temperature N_2 adsorption/desorption analysis indicate that sample YDN-2 has a greater BET pore surface area and BJH total pore volume but a smaller average pore size than those of sample YDN-1. Referring to the International Union of Pure and Applied Chemistry (IUPAC) classification, the N_2 adsorption/desorption curves of the two collected samples are of Type IV isotherms with noticeable hysteresis loops (SI Figure S1a). According to the shape of the hysteresis loops,[23] the pore type of sample YDN-1 belongs to H2 (ink bottle-shaped pore) and that of sample XWX is primarily H3 (plate-like pore) (SI Figure S1a). Moreover, the N_2 adsorption results also suggest that significant portions of the pores in the two samples are small (diameter <10 nm) (SI Figure S1b).

For the CH_4 and CO_2 adsorption measurements, the two samples were crushed into powder and sieved to 80 mesh (~180 μm), according to the standard (GB/T 35210.1−2017), for determination of methane isothermal adsorption in shale. First, isotherms of excess adsorption of CO_2 and CH_4 for the two powdered samples were recovered from the gravimetric method at 30 °C (303.15 K), indicating that the samples have a higher adsorption capacity for CO_2 than for CH_4 (SI Table S1; Figure 1). The Langmuir volume from

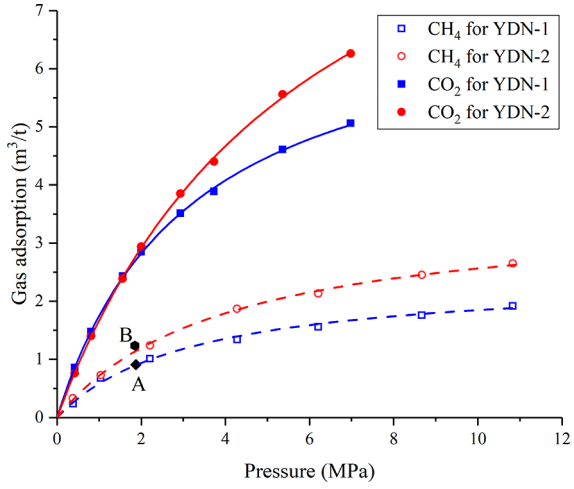

Figure 1. Adsorption isotherms for CO_2 and CH_4 in the two samples from gravimetric measurements.

excess adsorption is usually lower than that from absolute adsorption, but it still represents the relative adsorption capacity of CH_4 (or CO_2) among different samples at both subcritical and supercritical states of CH_4 (or CO_2).[24] The gravimetric method was employed in this study because it is less sensitive to the experimental environment and thus has higher precision than the volumetric method for isothermal adsorption experiments in shale.[25] Then, prior to the low-field NMR measurements, the prepared powders were dried at constant temperature (110 °C) for 1 h in a drying oven to remove moisture from the shale.

2.2. Low-Field NMR Experiments. *2.2.1. Experimental arrangement.* The ensemble experimental apparatus is modified from Liu et al.[20] and comprises a gas supply system, an NMR measurement apparatus, two core holders and a gas exhaust system (SI Figure S2). The gas supply system comprises three gas cylinders (CH_4, CO_2 and He) and a booster pump. The NMR measurement apparatus is a MiniMR-60 NMR spectrometer with a magnetic strength of 0.54 T at a frequency of 23.15 MHz using a 60 mm diameter magnet coil, which generates a homogeneous and stable field gradient. The two core holders are within a completely sealed environment for the sample cell and reference cell during the

DOI: 10.1021/acs.est.9b02432
Environ. Sci. Technol. 2019, 53, 9328−9336

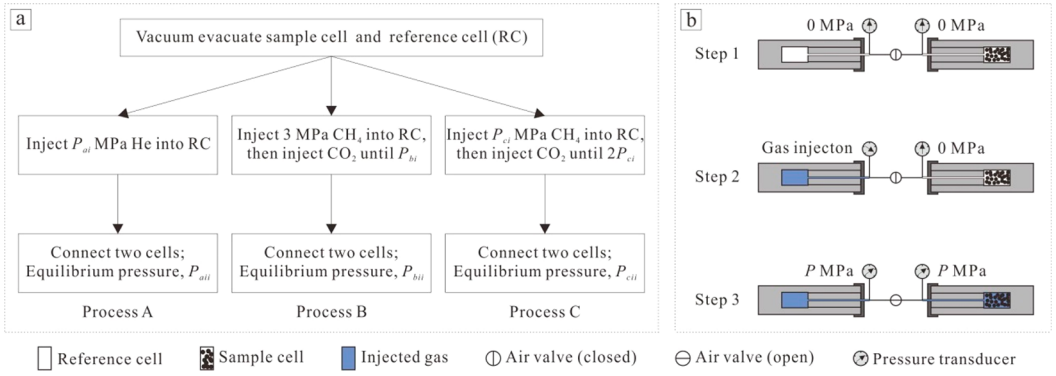

Figure 2. Experimental sequences used in this study. (a) Flow diagram of all experimental sequences; (b) Graphical representation for each experimental sequence. RC defines the reference cell, and P_{bi} and $2P_{ci}$ are the total pressures within the reference cell.

experiments, where the volume of both two cells is 62.78 cm^3. The temperature control device is a self-designed thermostat that is able to maintain the temperature in the sample and reference cells at a preset value. The gas exhaust system is constructed from a vacuum pump, a one-way release valve and an exhaust collector. Note that all the components placed in the magnet coil are specially designed with nonmetallic and nonmagnetic materials, including the sample cell, reference cell, thermostat and bodies of the two core holders. In addition, a temperature transducer and two high-precision pressure transducers are installed to monitor the temperature and gas pressure in the sample and reference cells with working intervals of 2 h in this study.

2.2.2. Mechanism of Low-Field NMR Relaxation. The NMR phenomenon results from the interaction between magnetic nuclei (e.g., hydrogen protons) and a magnetic field.[26,27] Hence, NMR relaxation is stimulated by CH_4 rather than by CO_2 (hydrogen-free), making it possible to identify CH_4 within a CH_4/CO_2 mixture. The number of hydrogen atoms present in the CH_4 molecule can be detected through the T_2 measurement.[28] In terms of a typical NMR measurement, total T_2 is related to surface relaxation affected by pore characteristics, bulk relaxation of fluid precession and diffusion relaxation caused by the gradient field.[29−31] Therefore, complete T_2 relaxation in porous media yields the following mathematical formula,[32]

$$\frac{1}{T_2} = \rho\left(\frac{S}{V}\right)_{pore} + \frac{1}{T_{2B}} + \frac{D(\gamma G T_E)^2}{12} \quad (1)$$

where ρ is the T_2 surface relaxivity, μm/ms; $(S/V)_{pore}$ is the surface area to volume ratio (specific surface area) of the pores filled with hydrogen-containing fluid, μm^{-1}; T_{2B} refers to the bulk relaxation time, ms; D is the molecular diffusion coefficient, cm^2/s; γ is the gyromagnetic ratio, rad/(s·T); G is the magnetic field gradient, Gs/cm; and T_E is the echo spacing (unit: ms) used in the Carr, Purcell, Meiboom and Gill (CPMG) pulse sequences.[33,34]

The low-field NMR measurements are completed under a homogeneous and stable field gradient such that parameter G in eq 1 is sufficiently small to be ignored.[35] Consequently, eq 1 becomes

$$\frac{1}{T_2} = \rho\left(\frac{S}{V}\right)_{pore} + \frac{1}{T_{2B}} \quad (2)$$

According to eq 2, the actual T_2 relaxation comprises both the surface relaxation of adsorbed CH_4 and the bulk relaxation of free (nonadsorbed) CH_4 in shale. Based on this principle, Yao et al.[21] characterized the multiphase CH_4 in shale and built the following correlation to calculate the content of adsorbed CH_4,

$$V_{ad} = 0.4207 \times T_{2A} \quad (3)$$

where V_{ad} is the volume of adsorbed CH_4 (cm^3) at standard temperature and pressure (STP) and T_{2A} is the T_2 amplitude motivated by the adsorbed CH_4 in shale. Based on the STP molar volume of a gas (22.4 L/mol), eq 3 has another form through unit conversion,

$$n_{ad} = 1.878 \times 10^{-5} \times T_{2A} \quad (4)$$

where n_A represents the amount of substance (AOS) of the adsorbed CH_4 (unit: mol).

Referring to eq 3, Yao et al.[21] successfully provided a new approach to measure the CH_4 adsorption capacity of shale using low-field NMR theory. Because the NMR measurements in both this study and that by Yao et al.[21] were completed with an identical experimental setup, eq 3 and eq 4 were also adopted in this study to quantify the adsorbed CH_4 in shale during the experiments.

2.3. Experimental Procedures and Computational Methods. The prepared powders were immediately transferred into the sample cell after drying. The measurements include three separate experimental processes (Figure 2a), among which each process comprises three sequential steps (Figure 2b). The first operation (Step 1) is uniform for all experiments and is to apply a vacuum to both the sample and the reference cells for 2 h to remove all residual gases from the cells and from the shale powders. Subsequently, the connection between the two cells is closed, and the individual cells are isolated. The remaining operations and corresponding computations for each experimental process are given below (Figure 2).

Process A (He Saturation−for Pore Volume). Saturation of the samples with inert and nonsorbing He defines the pore volumes in the two cells via gas compressibility.

(Step 2) Inject He into the reference cell at pressure P_{ai}. (Step 3) Connect the sample cell and reference cell until pressures in the two cells are equilibrated (marked as P_{aii}). A total of three experiments were conducted at three different pressure increments, where P_{ai} (i = 1−3) is 2, 4, and 6 MPa.

Considering its nonpolar and inert properties,[36] He is introduced in Process A to determine the free volume (V_{free}) in

DOI: 10.1021/acs.est.9b02432
Environ. Sci. Technol. 2019, 53, 9328−9336

the two cells, including the volume of the reference cell (V_{rc}), the volume in the connecting lines (V_{pipe}) and the bulk volume (V_{sc}) in the sample cell (interparticle and intraparticle porosity of the shale powders). From the ideal-gas equation, the average of three measurements is treated as the equivalent volume V_{free},

$$V_{free} = \frac{1}{3} \times \sum_{i=1}^{3} \frac{P_{ai} \times V_{rc} \times Z_{aii}}{P_{aii} \times Z_{ai}} \quad (5)$$

where Z_{ai} and Z_{aii} are the compression factors at P_{ai} and P_{aii}, respectively, and V_{rc} is standardized as 62.78 cm^3 (6.278 × 10^{-5} m^3) in this study. Referring to eq 5, the calculated V_{free} for samples YDN-1 and YDN-2 are 100.46 cm^3 and 101.38 cm^3, respectively.

Process B (Measurement of CO_2/CH_4 Competitive Adsorption at Constant CH_4 Mass and Variable CH_4/CO_2 Pressure Ratio). Evaluation of CO_2/CH_4 competitive adsorption behavior by increasing exposure to CO_2 at a constant mass of CH_4 in shale.

(Step 2) Inject CH_4 at 3 MPa into the reference cell and then continue to inject CO_2 until the total pressure in the reference cell reaches P_{bi}. (Step 3) Connect the sample cell and the reference cell and then allow pressures to equilibrate to P_{bii}. Then, perform a series of eight independent experiments, where P_{bi} (i = 1−8) is 3, 4, 5, 6, 7, 8, 9, and 10 MPa.

According to the volumetric method and low-field NMR results, the adsorbed CO_2 in the shale is defined as

$$n_{bii-CO_2} = \frac{P_{bi} \times V_{rc}}{Z_{bi} \times R \times T} - \frac{P_{bii} \times V_{free}}{Z_{bii} \times R \times T} - n_{bii-CH_4} \quad (6)$$

where $n_{bii\text{-}CO2}$ and $n_{bii\text{-}CH4}$ are the AOS of adsorbed CO_2 and CH_4, respectively, in the shale (unit: mol) at P_{bii}, and $n_{bii\text{-}CH4}$ can be obtained from eq 4 using NMR measurements. Z_{bi} and Z_{bii} are the compression factors at P_{bi} and P_{bii}, respectively. R is the gas constant, J/(mol·K), and T represents the temperature, K. Note that the volume of gas in the adsorbed phase is ignored.

In this experimental process, the partial pressures of CH_4 and CO_2 in the reference cell are approximately equivalent when P_{bi} is 6 MPa, forcing the competitive adsorption of CH_4 and CO_2 in the shale to proceed under identical conditions (same temperature and partial pressure). Here, we define the ratio of adsorbed CO_2 relative to CH_4 under identical conditions, as the CO_2/CH_4 competitive adsorption ratio in shale (abbreviated to CO_2/CH_4 CAR) is defined as

$$CAR = \frac{V_{ii-CO_2}}{V_{ii-CH_4}} \quad (7)$$

where $V_{ii\text{-}CO2}$ and $V_{ii\text{-}CH4}$ (unit: cm^3/g) are the STP volume of adsorbed CO_2 and CH_4 in shale under the same original temperature and partial pressure, respectively. In this study, the CO_2/CH_4 CAR is used as a criterion to assess the performance of shale in preferentially adsorbing CO_2 relative to CH_4.

Process C (Measurement of CO_2/CH_4 CAR at Equal Pressures of CH_4 and CO_2 at Variable Total Pressure). Characterization of the CO_2/CH_4 CAR under a range of different pressures.

(Step 2) Inject CH_4 into the reference cell at P_{ci} MPa followed by CO_2 injection until the total pressure in the reference cell is doubled to $2P_{ci}$. (Step 3) Connect the sample cell and the reference cell and allow the pressure to equilibrate in the two cells to P_{cii}. This process has four groups of independent measurements, in which P_{ci} (i = 1−4) is 1, 2, 4, and 5 MPa, respectively.

In this situation, the AOS of adsorbed CO_2 is

$$n_{cii-CO_2} = \frac{2P_{ci} \times V_{rc}}{Z_{ci} \times R \times T} - \frac{P_{cii} \times V_{free}}{Z_{cii} \times R \times T} - n_{cii-CH_4} \quad (8)$$

where $n_{cii\text{-}CO2}$ (or $n_{cii\text{-}CH4}$) is the AOS of adsorbed CO_2 (or CH_4) at P_{cii}, mol; and $n_{cii\text{-}CH4}$ is from NMR measurements based on eq 4. Z_{ci} and Z_{cii} are the compression factors at $2P_{ci}$ and P_{cii}, respectively.

In this study, samples YDN-1 and YDN-2, when placed in the sample cell, have masses of 31.58 and 30.71 g, respectively. Except for the oven-drying of the shale powders, all other operations were performed at a constant temperature of 30 °C (303.15 K), a preset value of the thermostat. The NMR measurements and equilibrium pressures were recorded only when the pressures in the sample and reference cells were identical and stable, with no variation within 2 h (i.e., the progress of adsorption is complete). Note the above novel NMR-based approach is regarded as a propagable methodology applicable to other gas reservoirs (e.g., coal) because it is not limited by shale properties, as well as to the adsorption measurement of multiple components from other ^{1}H-contained/^{1}H-free gas mixture (e.g., CH_4 and N_2).

3. RESULTS AND DISCUSSION

We explore the characteristics of CO_2/CH_4 competitive adsorption in shale based on the separate adsorption capacities of the collected shale samples to CH_4 and CO_2. These data are used to define EGR efficiency and CO_2 sequestration capacity in shale.

3.1. CH_4 Adsorption Capacity During CO_2−CH_4 Interaction. For typical low-field NMR measurements, the signal due to the adsorbed CH_4 in shale is on the order of T_2< ~ 1 ms.[20,21] During loading by Process B (fixed CH_4 mass and variable CO_2/CH_4 ratio), the T_2 amplitudes recorded from the adsorbed CH_4 decrease with increasing P_{bi} (Figure 3). In the observed low-field NMR results, the adsorbed CH_4 content declines with an increasing CO_2/CH_4 pressure ratio (Figure 4), indicating that CO_2 reduces the CH_4 adsorption capacity in shale, potentially by competing for a finite number of sorption

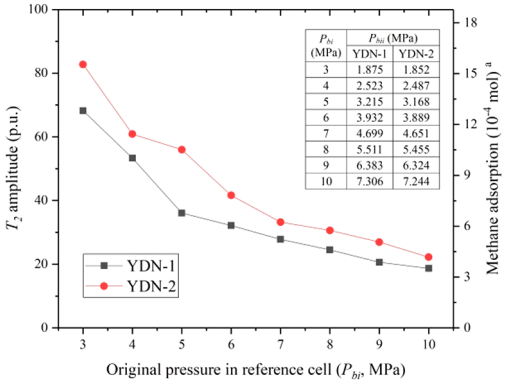

Figure 3. Low-field NMR measurements of adsorbed CH_4 in shale during experimental Process B (fixed CH_4 mass and variable CO_2/CH_4 ratio). P_{bii} is the equilibrium pressure is the stable pressure in the interconnected sample cell and reference cell. a, AOS of adsorbed CH_4 calculated from eq 4 using NMR.

DOI: 10.1021/acs.est.9b02432
Environ. Sci. Technol. 2019, 53, 9328−9336

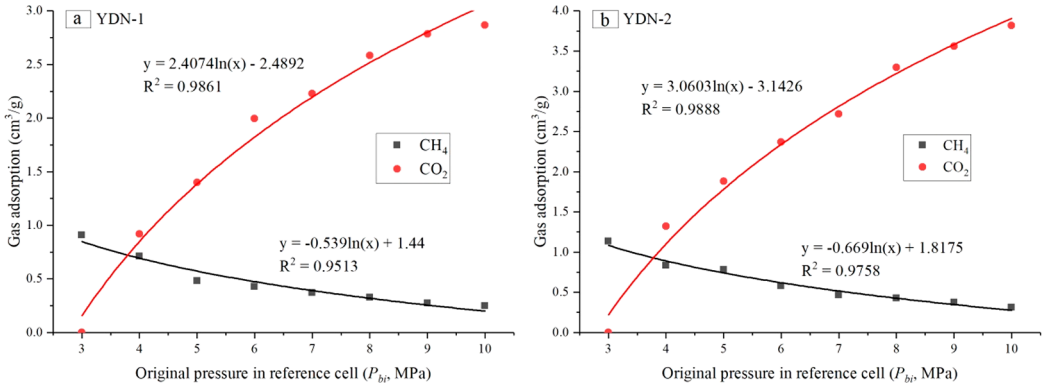

Figure 4. Adsorption capacity of CO_2 and CH_4 in Process B (fixed CH_4 mass and variable CO_2/CH_4 ratio). The quantification for adsorbed CH_4 and CO_2 is based on eqs 3) and (6), respectively. Note that the CO_2/CH_4 pressure ratio is approximately (P_{bi}-3)/3 with the partial pressure for CH_4 stabilized at 3 MPa in the reference cell.

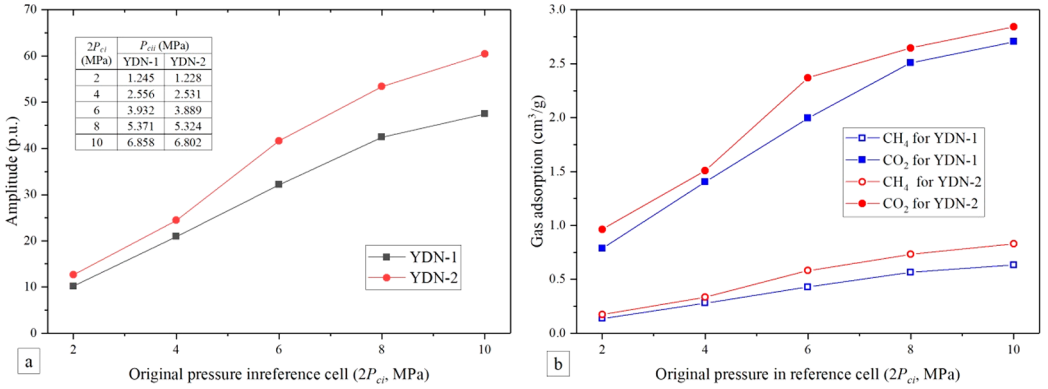

Figure 5. Measurements in experimental Process C (fixed CO_2/CH_4 pressure ratio). P_{cii} is the equilibrium pressure. (a) T_2 amplitudes resulting from adsorbed CH_4; (b) STP volume of adsorbed CH_4 and CO_2. The characterization for adsorbed CH_4 and CO_2 is based on eqs 3) and 8, respectively. The data at $2P_{ci}$ = 6 are from Process B when P_{bi} is 6 MPa (Figure 3; Figure 4).

sites. The STP volume of adsorbed CH_4 in sample YDN-1 varies from 0.909 cm^3/g before CO_2 injection (P_{bi} is 3 MPa) to 0.249 cm^3/g with a CO_2/CH_4 pressure ratio of ~7:3 when P_{bi} reaches 10 MPa (Figure 4a). For sample YDN-2, the STP volume of the adsorbed CH_4 decreases to 0.310 cm^3/g when P_{bi} is 10 MPa from an initial volume of 1.133 cm^3/g (P_{bi} = 3 MPa) (Figure 4b). The decreasing trends of CH_4 adsorption capacity with increasing CO_2 content for the two study samples yield a logarithmic relationship in P_{bi} (Figure 4).

In Process B (fixed CH_4 mass and variable CO_2/CH_4 ratio), the CH_4 adsorption in shale occurs in pure CH_4 before CO_2 injection (P_{bi} = 3 MPa). For sample YDN-1, the STP volume of the adsorbed CH_4 at the equilibrium pressure of 1.875 MPa (P_{bi} = 3 MPa, pure CH_4) is 0.909 cm^3/g (Figure 4), similar to that calculated by using the isothermal adsorption curve (Point A in Figure 1). Sample YDN-2 presents a similar behavior to that of YDN-1 before CO_2 injection (Point B in Figure 1), suggesting that low-field NMR may perform as a quantitative tool in determining the excess adsorption capacity of CH_4 in shale.

Process C (fixed CO_2/CH_4 pressure ratio) determines the variation in adsorbed CH_4 and CO_2 in shale when the CO_2/CH_4 pressure ratio is constant at ~1:1 but for different original total pressures, where the original partial pressures for CH_4 and CO_2 in the reference cell are approximately equivalent. The low-field NMR measurements (Figure 5a) show that the adsorbed CH_4 in the two samples increases with increasing $2P_{ci}$ (Figure 5b). This result occurs because both the partial pressure and concentration of CH_4 increase slightly with higher $2P_{ci}$ even as the CO_2/CH_4 pressure ratio remains constant.

In addition, in both Process B (fixed CH_4 mass and variable CO_2/CH_4 ratio) and Process C (fixed CH_4/CO_2 pressure ratio), the adsorbed CH_4 content in sample YDN-2 is greater than that in sample YDN-1 at the same pressure (Figure 4; Figure 5b). These results from sample YDN-2 exhibit a larger Langmuir volume of CH_4 ($V_{L\text{-}CH4}$) than those from sample YDN-1 (SI Table S1; Figure 1).

3.2. CO_2 Adsorption Capacity During CO_2–CH_4 Interaction. According to eq 6, the content of adsorbed CO_2 during Process B (fixed CH_4 mass and variable CH_4/CO_2 ratio) is shown in Figure 4. The STP volume of adsorbed CO_2 gradually reaches 2.868 cm^3/g after CO_2 access to sample YDN-1 (Figure 4a). The CO_2 volume finally increases to 3.819 cm^3/g as CO_2 is introduced into sample YDN-2 in Process B (Figure 4b). For the two study samples, the adsorbed CO_2 content increases logarithmically with increasing P_{bi} in the reference cell (namely, the increasing CO_2/CH_4 pressure ratio) (Figure 4) and implies that successive increments in adsorbed CO_2 in shale decrease at greater CO_2/CH_4 pressure ratios.

For Process C (fixed CO_2/CH_4 pressure ratio), the calculated content of adsorbed CO_2 is exhibited in Figure 5b. The adsorbed CO_2 in the two study samples increases monotonically when $2P_{ci}$ is increased from 2 to 10 MPa. The STP volumes of adsorbed CO_2 in samples YDN-1 and YDN-2

DOI: 10.1021/acs.est.9b02432
Environ. Sci. Technol. 2019, 53, 9328–9336

are 0.786 cm^3/g and 0.963 cm^3/g when $2P_{ci}$ is 2 MPa and increase to 2.704 cm^3/g and 2.843 cm^3/g ($2P_{ci}$ = 10 MPa), respectively (Figure 5b). This result is due to the higher partial pressure and concentration of CO_2 at greater $2P_{ci}$ even when the CO_2/CH_4 pressure ratio is constant.

In general, during experiments at either a constant mass of CH_4 (Process B) or a constant CO_2/CH_4 pressure ratio (Process C), sample YDN-2 exhibits a higher adsorbed CO_2 capacity than YDN-1 under the same environmental conditions (Figure 4; Figure 5b), this result is accorded to the higher Langmuir volume of CO_2 ($V_{L\text{-}CO2}$) for YDN-2 than for YDN-1 (SI Table S1; Figure 1).

3.3. Evaluation of CO_2/CH_4 CAR in Shale. In this study, CO_2/CH_4 *CAR* is used to describe the competitiveness of adsorbed CO_2 relative to CH_4 in shale when the original partial pressures of CO_2 and CH_4 are equivalent in the CO_2/CH_4 mixture. By definition, CO_2/CH_4 CAR = 1 represents an equal adsorption capacity for CO_2 and CH_4 with CO_2/CH_4 CAR > 1 representing an elevated adsorption capacity for CO_2 relative to CH_4.

Referring to eq 7, the CO_2/CH_4 CAR for the two samples is plotted in Figure 6. For sample YDN-1, the CO_2/CH_4 CAR is 5.81 at $2P_{ci}$ = 2 MPa and is 4.28 when $2P_{ci}$ increases to 10 MPa, indicating that the adsorption capacity for CO_2 is 5.81 times ($2P_{ci}$ = 2 MPa) and 4.28 times ($2P_{ci}$ = 10 MPa) greater than that for CH_4, respectively. For sample YDN-2, CO_2/CH_4 CAR decreases to 3.43 at $2P_{ci}$ = 10 MPa from 5.57 at the beginning ($2P_{ci}$ = 2 MPa) (Figure 6). Thus, CO_2/CH_4 CAR decreases with increasing pressures of CO_2 and CH_4, even though the CO_2/CH_4 pressure ratio is constant (~1:1). This result may occur because the increase in adsorbed CO_2 is larger than that in CH_4 at low pressure, and this gap diminishes at high pressure (Figure 7). This result implies that the increase in adsorbed CO_2 is more sensitive to pressure variation than that in adsorbed CH_4 at low pressure. Therefore, CO_2 occupies a greater proportion of adsorption sites than CH_4 at low pressure instead of at high pressure, resulting in a decrease in CO_2/CH_4 CAR with increasing $2P_{ci}$. Although this CAR tendency is obtained at gaseous state of CO_2 and CH_4 in this study, it corresponds with the variation simulated under supercritical conditions - CO_2/CH_4 CAR decreases with increasing pressure.[37,38] This indicates the change of CO_2/CH_4 CAR along with variable pressure complies with a similar law at both subcritical and supercritical states of CO_2 and CH_4.

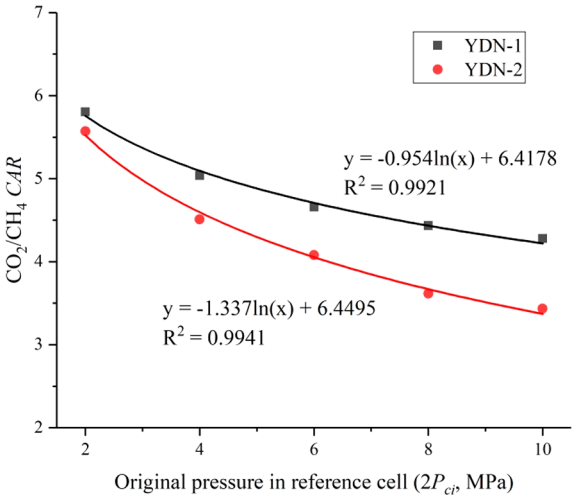

Figure 6. CO_2/CH_4 CAR in shale on the basis of experimental Process C (fixed CO_2/CH_4 pressure ratio). CAR represents the competitive adsorption ratio.

For the two collected samples, the downtrend of CO_2/CH_4 CAR correlates logarithmically with increasing pressure (Figure 6), suggesting that the decrease in CO_2/CH_4 CAR is more temperate at high pressure than at low pressure. From this requirement, if CO_2 has the same partial pressure as CH_4 in a CO_2/CH_4 mixture, the adsorption capacity of CO_2 relative to CH_4 is always superior when the total pressure ($2P_{ci}$) of CO_2 and CH_4 is less than 290 MPa for YDN-1 or 60 MPa for YDN-2.

In addition, sample YDN-1 exhibits an elevated CO_2/CH_4 CAR relative to sample YDN-2 (Figure 6), indicating that the competitiveness of adsorbed CO_2 relative to CH_4 in sample YDN-1 is usually stronger than that in sample YDN-2. This result may occur because the superior adsorptivity of CO_2 relative to CH_4 is more visible for shale with lower $V_{L\text{-}CO2}$ and $V_{L\text{-}CH4}$ (YDN-1) than for shale with higher $V_{L\text{-}CO2}$ and $V_{L\text{-}CH4}$ (YDN-2). However, further investigations are required to verify this speculation.

3.4. Implications for EGR Efficiency in Shale. Competitive adsorption between CO_2 and CH_4 enables EGR from the replacement of adsorbed CH_4 by injected CO_2 in shale.[13] For measurements at constant CH_4 mass (Process B), the content of adsorbed CH_4 gradually declines with respect to

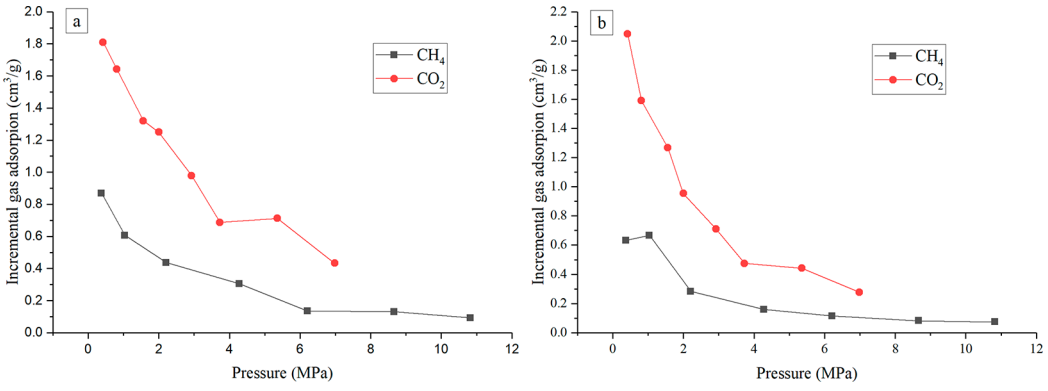

Figure 7. Variation in incremental gas adsorption at different pressures. a, sample YDN-1; b, sample YDN-2. Source data are obtained from the adsorption isotherms of CO_2 and CH_4 in Figure 1.

DOI: 10.1021/acs.est.9b02432
Environ. Sci. Technol. 2019, 53, 9328−9336

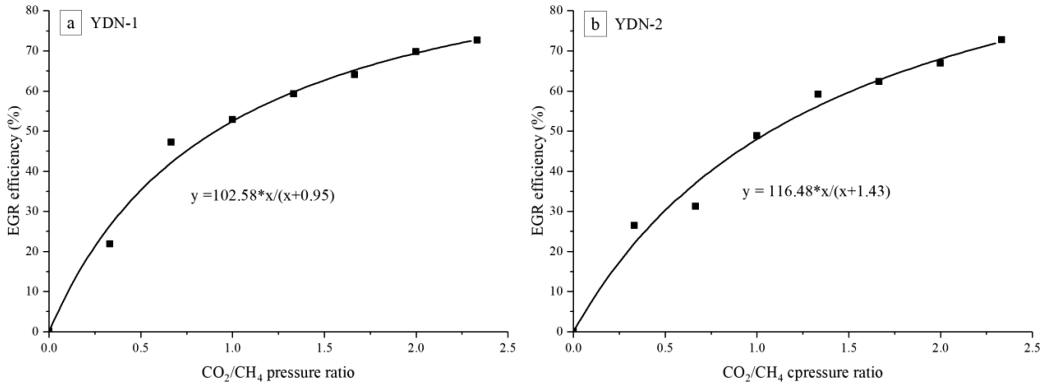

Figure 8. EGR efficiency during experimental Process B (fixed CH_4 mass and variable CO_2/CH_4 ratio). EGR represents enhanced gas recovery.

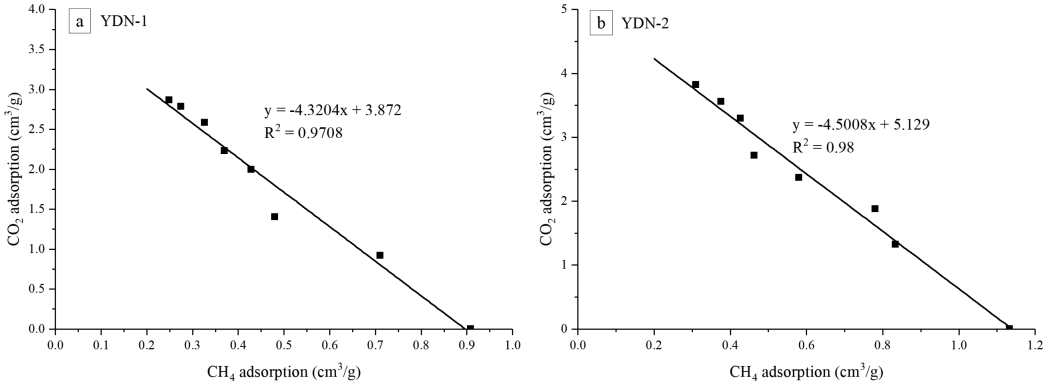

Figure 9. Relationship between adsorbed content of CO_2 and CH_4 during experimental Process B (fixed CH_4 mass and variable CO_2/CH_4 ratio).

the increasing CO_2/CH_4 pressure ratio, signaling enhanced recovery of adsorbed CH_4 caused by CO_2 preferential adsorption (Figure 4). Therefore, EGR efficiency in this study is defined as

$$\text{EGR efficiency} = \frac{V_{\text{original}} - V_{\text{residual}}}{V_{\text{original}}} \times 100\% \quad (9)$$

where V_{original} represents the original adsorbed CH_4 volume (cm^3/g) without CO_2 injection, while V_{residual} represents the residual volume (cm^3/g) of adsorbed CH_4 after CO_2 displacement. Taking sample YDN-2 as an example, the adsorbed CH_4 content is 1.133 cm^3/g without CO_2 injection and decreases to 0.310 cm^3/g at P_{bi} = 10 MPa (Figure 4b), suggesting that 72.64% of the adsorbed CH_4 is displaced by the sorbing CO_2. The EGR efficiencies for the two samples are illustrated in Figure 8 for different P_{bi}.

The EGR efficiency for the two samples varies with increasing CO_2/CH_4 pressure ratio according to a Langmuir-like function (Figure 8), asymptoting to a maximum efficiency at high pressure ratios. Therefore, the EGR efficiency in a particular shale may be estimated from the CO_2/CH_4 pressure ratio. For instance, to achieve an 80% EGR efficiency of adsorbed CH_4 in sample YDN-1, the CO_2/CH_4 pressure ratio can be projected to be 3.3658 (Figure 8a). This finding implies that if the original partial pressure of injected CO_2 is 3.3658 times higher than that of adsorbed CH_4 in sample YDN-1, then 80% of the original adsorbed CH_4 would be replaced by CO_2. Hereby, these results would be helpful to accurately predict the EGR performance and determine an appropriate pressure during potential CCGS operations in shale reservoirs.

3.5. Implications for CO_2 Sequestration in Shale.

Shale-based CCGS techniques enable underground storage of CO_2 as an adsorbed phase on the surface of kerogen or other minerals (e.g., clay minerals), as a free phase within fractures and intergranular porosity and as a dissolved phase in formation fluids.[7,8,39] In this study, we focus exclusively on CO_2 sequestration in the adsorbed phase, where some of the free CO_2 is transferred to the adsorbed phase after replacing CH_4 on adsorption sites during competitive adsorption.

For sorption measurements at a constant CH_4 mass (Process B), the adsorption capacity for CO_2 increases and that for CH_4 decreases with increasing pressure (Figure 4). Figure 9 shows the relationship between the adsorption capacities of CO_2 and CH_4 in shale during sorption at a constant CH_4 mass (Process B), showing an inverse linear correlation for both study samples. Accordingly, before the adsorbed CH_4 is entirely replaced by CO_2, the adsorbed CO_2 may be estimated using the residual content of adsorbed CH_4 during CO_2−CH_4 competitive adsorption in shale. The capacity for CO_2 sequestration in the adsorbed phase is ~3.87 cm^3/g for sample YDN-1 and ~5.13 cm^3/g for sample YDN-2 (Figure 9), and the EGR efficiency of the adsorbed CH_4 may approach 100%.

In reality, the EGR efficiency may only approach 100%; thus, the capacity of CO_2 sequestration in the adsorbed phase is considered as the theoretical maximum when the residual content of adsorbed CH_4 tends to 0 cm^3/g. Furthermore, compared with sample YDN-1, sample YDN-2 has a greater capacity of CO_2 sequestration, probably resulting from its greater $V_{L\text{-}CO2}$ (SI Table S1; Figure 1). In addition, the theoretical maximum capacity of CO_2 sequestration in adsorbed phase for two samples in this study is lower than

DOI: 10.1021/acs.est.9b02432
Environ. Sci. Technol. 2019, 53, 9328−9336

their $V_{L\text{-}CO2}$ respectively (SI Table S1), which means the CO_2 sequestration capacity during CO_2-EGR process in shale tends to be overestimated if the $V_{L\text{-}CO2}$ is adopted in CO_2 storage evaluation. Therefore, the estimation method about CO_2 sequestration in this work would be useful to accurately predict the potential of CO_2 storage during CO_2/CH_4 competitive adsorption in shale.

■ ASSOCIATED CONTENT

Supporting Information

The Supporting Information is available free of charge on the ACS Publications website at DOI: 10.1021/acs.est.9b02432.

Information on the low-temperature (77 K) N_2 adsorption/desorption analysis of two samples (Figure S1), schematic diagram of the experimental arrangement (Figure S2,) and the basic properties of the collected shale samples (Table S1) (PDF)

■ AUTHOR INFORMATION

Corresponding Author

*Phone: 86-28-62138375; e-mail: j.liu@scu.edu.cn.

Present Address

‖(J.L.) Institute of New Energy and Low-Carbon Technology, Sichuan University, No.24 South Section 1, Yihuan Road, Chengdu 610065, China.

Notes

The authors declare no competing financial interest.

■ ACKNOWLEDGMENTS

We acknowledge financial support from the National Natural Science Foundation of China (11872258) and the Science & Technology Department of Sichuan Province (19GJHZ0146).

■ REFERENCES

(1) Elliot, T. R.; Celia, M. A. Potential restrictions for CO_2 sequestration sites due to shale and tight gas production. *Environ. Sci. Technol.* **2012**, *46* (7), 4223−4227.

(2) Liu, Y. Y.; Wilcox, J. Molecular simulation studies of CO_2 adsorption by carbon model compounds for carbon capture and sequestration applications. *Environ. Sci. Technol.* **2013**, *47*, 95−101.

(3) Tao, Z. Y.; Clarens, A. Estimating the carbon sequestration capacity of shale formations using methane production rates. *Environ. Sci. Technol.* **2013**, *47* (19), 11318−11325.

(4) Merey, S. Analysis of the effect of experimental adsorption uncertainty on CH_4 production and CO_2 sequestration in Dadas shale gas reservoir by numerical simulations. *J. Pet. Sci. Eng.* **2019**, *178*, 1051−1066.

(5) Louk, K.; Ripepi, N.; Luxbacher, K.; Gilliland, E.; Tang, X.; Keles, C.; Schlosser, C.; Diminick, E.; Keim, S.; Amante, J.; Micheal, K. Monitoring CO_2 storage and enhanced gas recovery in unconventional shale reservoirs: results from the Morgan County, Tennessee injection test. *J. Nat. Gas Sci. Eng.* **2017**, *45*, 11−25.

(6) Fathi, E.; Akkutlu, I. Y. Multi-component gas transport and adsorption effects during CO_2 injection and enhanced shale gas recovery. *Int. J. Coal Geol.* **2014**, *123*, 52−61.

(7) Kim, T. H.; Cho, J.; Lee, K. S. Evaluation of CO_2 injection in shale gas reservoirs with multi-component transport and geomechanical effects. *Appl. Energy* **2017**, *190*, 1195−1206.

(8) Godec, M.; Koperna, G.; Petrusak, R.; Oudinot, A. Potential for enhanced gas recovery and CO_2 storage in the Marcellus shale in the Eastern United States. *Int. J. Coal Geol.* **2013**, *118*, 95−104.

(9) Edwards, R. W.; Celia, M. A.; Bandilla, K. W.; Doster, F.; Kanno, C. M. A model to estimate carbon dioxide injectivity and storage capacity f-or geological sequestration in shale gas wells. *Environ. Sci. Technol.* **2015**, *49* (15), 9222−9229.

(10) Wang, T. Y.; Tian, S. C.; Li, G. S.; Sheng, M. Selective adsorption of supercritical carbon dioxide and methane binarymixture in shale kerogen nanopores. *J. Nat. Gas Sci. Eng.* **2018**, *50*, 181−188.

(11) Song, R.; Cui, M. Molecular simulation on competitive adsorption mechanism of CH_4/CO_2 on shale kerogen. *Arabian J. Geosci.* **2018**, *11*, 408.

(12) Zhang, H. B.; Cao, D. P. Molecular simulation of displacement of shale gas by carbon dioxide at different geological depths. *Chem. Eng. Sci.* **2016**, *156* (15), 121−127.

(13) Huang, L.; Ning, Z. F.; Wang, Q.; Zhang, W. T.; Cheng, Z. L.; Wu, X. I.; Qin, H. B. Effect of organic type and moisture on CO_2/CH_4, competitive adsorption in kerogen with implications for CO_2 sequestration and enhanced CH_4 recovery. *Appl. Energy* **2018**, *210*, 28−43.

(14) Gasparik, M.; Ghanizadeh, A.; Bertier, P.; Gensterblum, Y.; Bouw, S.; Krooss, B. M. High-pressure methane sorption isotherms of black shales from the Netherlands. *Energy Fuels* **2012**, *26* (8), 4995−5004.

(15) Duan, S.; Min, G.; Du, X. D.; Xian, X. F. Adsorption equilibrium of CO_2 and CH_4 and their mixture on sichuan basin shale. *Energy Fuels* **2016**, *30* (3), 2248−2256.

(16) Qi, R. R.; Ning, Z. F.; Wang, Q.; Zeng, Y.; Huang, L.; Zhang, S.; Du, H. M. Sorption of methane, carbon dioxide, and their mixtures on shales from Sichuan basin, China. *Energy Fuels* **2018**, *32* (3), 2926−2940.

(17) Nuttall, B.; Eble, C. F.; Drahovzal, J. A.; Bustin, M. Analysis of Devonian Black Shales for Potential Carbon Dioxide Sequestration and Enhanced Natural Gas Production. *Report DE-FC26−02NT41442 Prepared by the Kentucky Geological Survey*; University of Kentucky, for the U.S. Department of Energy, National Energy Technology Laboratory, 2005.

(18) Chareonsuppanimit, P.; Mohammad, S. A.; Robinson, R. L., Jr.; Gasem, K. A. M. Highpressure adsorption of gases on shales: measurements and modeling. *Int. J. Coal Geol.* **2012**, *95*, 34−46.

(19) Merey, S.; Sinayuc, C. Analysis of carbon dioxide sequestration in shale gas reservoirs by using experimental adsorption data and adsorption models. *J. Nat. Gas Sci. Eng.* **2016**, *36* (Part A), 1087−1105.

(20) Liu, J.; Yao, Y. B.; Liu, D. M.; Elsworth, D. Experimental evaluation of CO_2 enhanced recovery of adsorbed-gas from shale. *Int. J. Coal Geol.* **2017**, *179*, 211−218.

(21) Yao, Y. B.; Liu, J.; Liu, D. M.; Chen, J. Y.; Pan, Z. J. A new application of NMR in characterization of multiphase methane and adsorption capacity of shale. *Int. J. Coal Geol.* **2019**, *201*, 76−85.

(22) Chen, L.; Lu, Y. C.; Jiang, S.; Li, J. Q.; Guo, T. L.; Luo, C. Heterogeneity of the lower silurianlongmaxi marine shale in the southeast Sichuan basin of China. *Mar. Pet. Geol.* **2015**, *65*, 232−246.

(23) Sing, K. S. W.; Everett, D. H.; Haul, R. A. W.; Moscou, L.; Pierotti, R. A.; Rouquerol, J.; Siemieniewsha, T. Reporting physisorption data for gas/solid systems with special reference to the determination of surface area and porosity. *Pure Appl. Chem.* **1985**, *57*, 603−619.

(24) Zhou, S. W.; Xue, H. Q.; Ning, Y.; Guo, W.; Zhang, Q. Experimental study of supercritical methane adsorption in Longmaxi shale: Insights into the density of adsorbed methane. *Fuel* **2018**, *211*, 140−148.

(25) Zhou, S. W.; Li, Q.; Xue, H. Q.; Guo, W.; Li, X. B.; Lu, B. Comparative study on the volumetric and gravimetric method forisothermal adsorption experiment of shale. *Chem. Ind. Eng. Prog.* **2017**, *36* (5), 1690−1697.

(26) Darrow, K. K. Magnetic resonance: part I - nuclear magnetic resonance. *Bell Syst. Tech. J.* **1953**, *32* (1), 74−99.

(27) Hazlewood, C. F.; Chang, D. C.; Nichols, B. L.; Woessner, D. E. Nuclear magnetic resonance transverse relaxation times of water protons in skeletal muscle. *Biophys. J.* **1974**, *14* (8), 583−606.

(28) Seevers, D. O., A nuclear magnetic method for determining the permeability of sandstones, *Paper L. SPWLA 7th Annual Logging*

DOI: 10.1021/acs.est.9b02432
Environ. Sci. Technol. 2019, 53, 9328−9336

Symposium, 9−11 May, Society of Professional Well Log Analysts Transactions, Tulsa, OK, 1−14. 1966.
(29) Kleinberg, R. L.; Vinegar, H. J. NMR Properties of Reservoir Fluids. *Log Analyst* **1996**, *37* (6), 20−32.
(30) Straley, C.; Rossini, D.; Vinegar, H.; Tutunjian, P.; Morriss, C. Core analysis by low field NMR. *Log Analyst* **1997**, *38* (2), 84−94.
(31) Coates, G. R.; Xiao, L. Z.; Prammer, M. G. *NMR Logging Principles and Applications*; Gulf Publishing Company: Houston, TX. 1999.
(32) Tan, M. J.; Mao, K. Y.; Song, X. D.; Yang, X.; Xu, J. J. NMR petrophysical interpretation method of gas shale based on core NMR experiment. *J. Pet. Sci. Eng.* **2015**, *136*, 100−111.
(33) Carr, H. Y.; Purcell, E. M. Effects of diffusion on free precession in nuclear magnetic resonance experiments. *Phys. Rev.* **1954**, *94* (3), 630−638.
(34) Meiboom, S.; Gill, D. Modified Spin-Echo method for measuring nuclear relaxation times. *Rev. Sci. Instrum.* **1958**, *29* (8), 688−691.
(35) Yao, Y. B.; Liu, D. M.; Xie, S. B. Quantitative characterization of methane adsorption on coal using a low-field NMR relaxation method. *Int. J. Coal Geol.* **2014**, *131*, 32−40.
(36) Starzewski, P.; Zielenkiewicz, W. DSC-TG studies of coal structure modification by the inert gas Helium. *Thermochim. Acta* **1990**, *160* (2), 215−222.
(37) Zhou, W. N.; Wang, H. B.; Yan, Y. Y.; Liu, X. L. Adsorption mechanism of CO_2/CH_4 in kaolinite clay: Insight from molecular simulation. *Energy Fuels* **2019**, 336542.
(38) Wang, X. Q.; Zhai, Z. Q.; Jin, X.; Wu, S. T.; Li, J. M.; Sun, L.; Liu, X. D. Molecular simulation of CO_2 /CH_4 competitive adsorption in organic matter pores in shale under certain geological conditions. *Petrol. Explor. Dev+.* **2016**, *43* (5), 841−848.
(39) Wang, T. Y.; Tian, S. C.; Li, G. S.; Sheng, M.; Ren, W. X.; Liu, Q. L.; Zhang, A. K. Molecular Simulation of CO_2/CH_4 Competitive Adsorption on Shale Kerogen for CO_2 Sequestration and Enhanced Gas Recovery. *J. Phys. Chem. C* **2018**, *122*, 17009−17018.

DOI: 10.1021/acs.est.9b02432
Environ. Sci. Technol. 2019, 53, 9328−9336